1-1-2013

In vivo magnetic resonance imaging of glucose - initial experience

Hyla Allouche-Arnon
Hadassah University Medical Centre

Trevor Wade
Western University

Lanette Friesen Waldner
Western University

Valentina N. Miller
Hadassah University Medical Centre

J. Moshe Gomori
Hadassah University Medical Centre

See next page for additional authors

CONTRAST MEDIA & MOLECULAR IMAGING

Received: 16 October 2011, Revised: 16 July 2012, Accepted: 27 July 2012, Published online in Wiley Online Library: 2012

(wileyonlinelibrary.com) DOI: 10.1002/cmmi.1497

In vivo magnetic resonance imaging of glucose – initial experience

Hyla Allouche-Arnon[a,b†], Trevor Wade[c,d†], Lanette Friesen Waldner[c,d], Valentina N. Miller[a], J. Moshe Gomori[a,b]*, Rachel Katz-Brull[a,b‡] and Charles A. McKenzie[c,d‡]

A new noninvasive, nonradioactive approach for glucose imaging using spin hyperpolarization technology and stable isotope labeling is presented. A glucose analog labeled with ^{13}C at all six positions increased the overall hyperpolarized imaging signal; deuteration at all seven directly bonded proton positions prolonged the spin–lattice relaxation time. High-bandwidth ^{13}C imaging overcame the large glucose carbon chemical shift dispersion. Hyperpolarized glucose images in the live rat showed time-dependent organ distribution patterns. At 8 s after the start of bolus injection, the inferior vena cava was demonstrated at angiographic quality. Distribution of hyperpolarized glucose in the kidneys, vasculature, and heart was demonstrated at 12 and 20 s. The heart-to-vasculature intensity ratio at 20 s suggests myocardial uptake. Cancer imaging, currently performed with ^{18}F-deoxyglucose positron emission tomography (FDG-PET), warrants further investigation, and glucose imaging could be useful in a vast range of clinical conditions and research fields where the radiation associated with the FDG-PET examination limits its use. Copyright © 2012 John Wiley & Sons, Ltd.

Keywords: carbon-13; deuterium; hyperpolarization; uptake; 3 T; rat; DNP

1. INTRODUCTION

Glucose is probably the most researched biochemical since fermentation was studied by Louis Pasteur (1) and glycolysis was eventually delineated by Otto Meyerhof and colleagues (2). Current glucose research includes studies of transporters and metabolic enzymes at the molecular level, and translational studies related to diabetes, inflammation and cancer (3).

In clinical imaging, the radioactive glucose analog ^{18}F-deoxyglucose (FDG) is routinely used in positron emission tomography (PET) imaging procedures for identifying primary and metastatic tumors. FDG-PET imaging is important in determining the extent of disease, and influences treatment decisions. Recently, FDG-PET has been shown to have high sensitivity for inflammation, specifically for identifying the origin of fever of unknown origin (4). However, radiation exposure associated with FDG-PET studies limits repeat examinations, precludes imaging of children and pregnant women except in unusual circumstances, and prevents the use of this valuable imaging technique in humans for wide-ranging research relating to brain function in health and disease and to glucose utilization in bodily organs *in situ*.

Nonradioactive analogs of glucose, labeled with the stable isotope carbon-13, have been used in the last three decades to study glucose metabolism in tissue culture, small animals and humans with the aid of the noninvasive technology of magnetic resonance spectroscopy (MRS) (5–11). Glucose analogs and derivatives labeled with both carbon-13 and deuterium have also been used to monitor glucose metabolism *ex vivo*. For example, [1-^{13}C]glucose and [6,6-$^{2}H_2$]glucose were utilized as a means to monitor human glucose metabolism (12). The metabolic products of these labeled glucose analogs were assayed in body fluids by means of gas chromatography combined with mass spectrometry. In another study [1,6-$^{13}C_2$]glucose with or without deuterium labeling (D16) was used to monitor glucose metabolism in humans by NMR spectroscopy of blood and urine samples (13). Glucose analogs labeled with stable isotopes have also been used to study glucose metabolism noninvasively in animals and humans (14).

Recent advances in spin hyperpolarization (15–17) raised hopes for noninvasive and nonradioactive glucose imaging and monitoring of metabolism using MRI. However, it was found that the T_1 of glucose carbons is <2 s which is prohibitively short for hyperpolarized MRI applications (18). Capitalizing on our experience with new molecular imaging agents for the hyperpolarized MR technology using deuteration of sp3 carbon-13 positions

* *Correspondence to: J. Moshe Gomori, Department of Radiology, Hadassah – Hebrew University Medical Center, Jerusalem, Israel. E-mail: gomori@cc.huji.ac.il*

† *Hyla Allouche-Arnon and Trevor Wade contributed equally.*

‡ *Rachel Katz-Brull and Charles A. McKenzie contributed equally.*

a *H. Allouche-Arnon, V. N. Miller, J. M. Gomori, R. Katz-Brull Department of Radiology, Hadassah - Hebrew University Medical Center, Jerusalem, Israel*

b *H. Allouche-Arnon, J. M. Gomori, R. Katz-Brull BrainWatch Ltd, Tel-Aviv, Israel*

c *T. Wade, L. F. Waldner, C. A. McKenzie Department of Medical Biophysics, The University of Western Ontario, London, Ontario, Canada*

d *T. Wade, L. F. Waldner, C. A. McKenzie Robarts Research Institute, The University of Western Ontario, London, Ontario, Canada*

(19,20), we show here that direct glucose imaging is feasible *in vivo*, by MRI, using a glucose analog that is labeled with stable, nonradioactive isotopes. This analog, [U-$^{13}C_6$, $^{2}H_7$]glucose, is enriched with carbon-13 in all carbon positions and enriched with deuterium atoms in all proton positions that are directly bonded to carbons. We show that this strategy allows nonradioactive, noninvasive imaging of glucose with an off-the-shelf compound.

2. RESULTS

To capitalize on the DNP spin polarization technology for glucose imaging, the T_1s of the glucose carbons must be long enough to provide a sufficient temporal window for observing the hyperpolarized state in a living subject. The T_1 of the glucose carbon-13 nuclei was previously reported to be <2 s for all carbon positions, making glucose unsuitable for use with the DNP technique (18). Our studies confirmed this finding, showing an average T_1 for native glucose carbons of 1.6 ± 0.4 s (mean standard deviation) for a 400 mM solution in water at 11.8 T and 37 °C. To further study the suitability of glucose for the DNP technique, we investigated the effects of sp3 carbon deuteration (19), that is, substitution of directly bonded hydrogen(s) by deuterium atoms for a tetrahedrally coordinated carbon, on the T_1 of these carbons. Deuteration was found to prolong the T_1 of these sp3 carbons but other factors such as concentration, magnetic field and directly bonded- or adjacent carbon-13 nuclei were found to influence this relaxation time as well, as described below. We have investigated the possible effects of these factors in order to guide utilization of glucose's sp3 carbon deuteration in various potential hyperpolarized glucose MR applications including imaging and spectroscopy.

2.1. Concentration and Osmolarity

The effect of high [U-$^{13}C_6$, $^{2}H_7$]glucose concentration on the T_1 of glucose carbon positions was first investigated at 7 and 11.8 T (Fig. 1 and Table 1) under thermal equilibrium conditions. The T_1 of glucose carbons was found to be longer in a 400 mM solution compared with a 10-fold concentrated solution (4.03 M) at both magnetic fields. The mean difference between the T_1 values for the two concentrations was 6.9 ± 1.4 s (4.0 ± 0.5 vs 10.9 ± 1.7 s, a 174% increase) and 4.5 ± 1.4 s (4.4 ± 0.4 vs 8.9 ± 1.5 s, a 103% increase) at 7 and 11.8 T, respectively. The mean T_1s and standard deviations were calculated from the data obtained for eight groups of signals as shown in Fig. 2 and summarized in Table 1.

High osmolality media are typically in the range of 5–8 times the osmolality of plasma (21), that is, not above ca. 2.4 M. Therefore, the 4.03 M solution is too concentrated to serve as a contrast medium. However, the 400 mM solution can be considered to be in the range of iso-osmolar to low-osmolality contrast medium, whereas such low-osmolality media typically have up to 2–3 times the osmolality of plasma (21), that is, 600–900 mM. The above findings therefore suggested that iso- to low-osmolality conditions are favorable for T_1 prolongation, and that hyperpolarized glucose media should not be kept at high osmolarity during transfer of hyperpolarized glucose from the polarizer to the subject and administration to the subject.

The effect of concentration was further investigated in a solution of 40 mM [U-$^{13}C_6$, $^{2}H_7$]glucose in water at 11.8 T. The T_1 was found to be longer at the lower dilution (Table 1 and Fig. 1). The mean difference between the T_1 values at 400 and 40 mM was 6.5 ± 1.8 s (8.9 ± 1.5 s at 400 mM vs 15.4 ± 1.8 s at 40 mM, a 74% increase). However, when the osmolarity of the 40 mM solution was raised to 400 mOsm (by addition of sodium chloride), the T_1 of glucose carbons decreased to 12.5 ± 1.3 s (41% decrease) yet remained above that of glucose carbons in the 400 mM glucose solution (Table 1 and Fig. 1). Further investigation into the effect of concentration and solutes on the T_1 of [U-$^{13}C_6$, $^{2}H_7$]glucose carbons is underway.

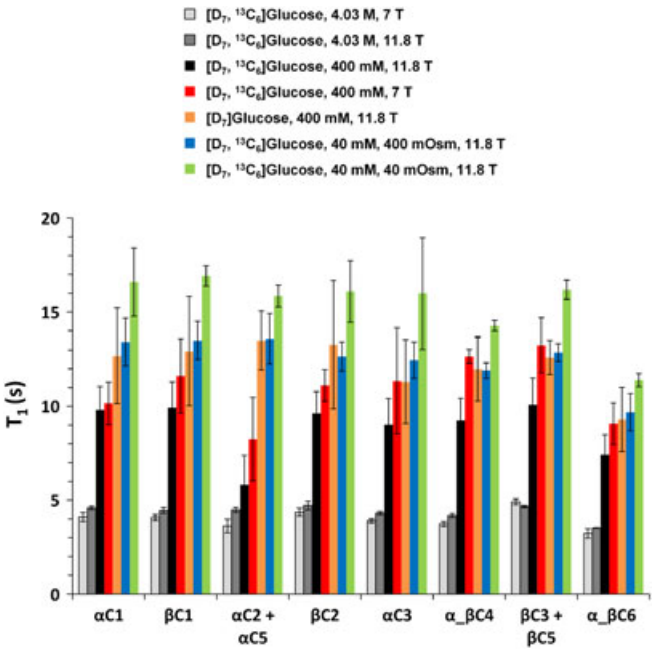

Figure 1. T_1 of ^{13}C nuclei in deuterated glucose molecules. The labels $C_i\alpha$ and $C_i\beta$ mark the signals of the glucose carbon at position i in the α and β anomers, respectively. The studies were carried out at 37 °C. All solutions were made in purified water containing 10% D_2O. The error bars represent the 95% confidence interval as determined by the inversion-recovery curve fitting. The exact values for each position are given in detail in Table 1 and in the text. These varied conditions provide means to assess the effect of concentration, osmolarity, magnetic field strength and ^{13}C–^{13}C dipolar interactions on the T_1 of the various ^{13}C nuclei.

2.2. Magnetic Field Strength

The effect of magnetic field strength on the T_1 of [U-$^{13}C_6$, $^{2}H_7$] glucose carbons was investigated at 7, 11.8 and 4.7 T under thermal equilibrium conditions (400 mM in water, 37 °C), as well as at 3 T, in a hyperpolarized state. The T_1 of [U-$^{13}C_6$, $^{2}H_7$]glucose carbons was longer at 7 T compared with 11.8 T (Fig. 1 and Table 1), with a mean difference of 2.4 $\pm$1.6 s between both fields (11.2 ± 1.6 vs 8.9 ± 1.5 s).

Figure 2 shows the structure of the [U-$^{13}C_6$, $^{2}H_7$]-D-glucose α and β anomers and the various carbon positions and deuteration sites therein. The ^{13}C spectrum of this molecule at 11.8 T is shown with assignment for the eight main groups of signals observed. At 7 T, these eight groups of signals are resolved as well. However, at 4.7 T the five signal groups between 70 and 80 ppm overlap. Nevertheless, positions 1 and 6 could be resolved and showed T_1 values of 8.3 and 6.2 s, respectively (Table 1).

Table 1. T_1 of ^{13}C nuclei in deuterated glucose

		T_1 at position and anomer (s)[a]							
	Molecule and conditions	$C_1\alpha$	$C_1\beta$	$(C_2+C_5)\alpha$	$C_2\beta$	$C_3\alpha$	$C_4(\alpha+\beta)$	$(C_3+C_5)\beta$	$C_6(\alpha+\beta)$
A	[U-$^{13}C_6$, $^2H_7$]glucose, 7 T, 4.03 M, 4.03 Osm, TE	4.1 (3.9, 4.3)	4.1 (3.9, 4.2)	3.6 (3.2, 4.0)	4.4 (4.1, 4.6)	3.9 (4.8, 4.0)	3.7 (3.6, 3.9)	4.9 (4.8, 5.1)	3.2 (3.0, 3.5)
B	[U-$^{13}C_6$, $^2H_7$]glucose, 11.8 T, 4.03 M, 4.03 Osm, TE	4.6 (4.5, 4.7)	4.5 (4.3, 4.6)	4.5 (4.3, 4.6)	4.7 (4.5, 4.9)	4.3 (4.2, 4.4)	4.2 (4.1, 4.3)	4.7 (4.6, 4.7)	3.5 (3.5, 3.5)
C	[U-$^{13}C_6$, $^2H_7$]glucose, 11.8 T, 400 mM, 400 mOsm, TE	9.8 (8.6, 11.1)	9.9 (8.6, 11.3)	5.8 (4.2, 7.4)	9.6 (8.5, 10.8)	9.0 (7.6, 10.4)	9.3 (8.1, 10.4)	10.1 (8.7, 11.5)	7.4 (6.4, 8.5)
D	[U-$^{13}C_6$, $^2H_7$]glucose, 7 T, 400 mM, 400 mOsm, TE	10.2 (9.0, 11.3)	11.6 (9.6, 13.6)	8.3 (6.0, 10.5)	11.1 (10.3, 12.0)	11.4 (8.5, 14.2)	12.7 (12.3, 13.0)	13.2 (11.8, 14.7)	9.1 (8.0, 10.2)
E	[$^2H_7$]glucose, 11.8 T, 400 mM, 400 mOsm, TE	12.7 (10.1, 15.2)	12.9 (10.0, 15.8)	13.5 (11.9, 15.0)	13.3 (9.9, 16.7)	11.3 (9.1, 13.5)	12.0 (10.3, 13.7)	12.6 (11.7, 13.5)	9.3 (7.6, 11.0)
F	[U-$^{13}C_6$, $^2H_7$]glucose, 11.8 T, 40 mM, 400 mOsm, TE	13.4 (12.2, 14.7)	13.5 (12.5, 14.5)	13.6 (12.3, 14.9)	12.7 (11.9, 13.4)	12.5 (11.5, 13.4)	11.9 (11.5, 12.3)	12.9 (12.4, 13.3)	9.7 (8.7, 10.7)
G	[U-$^{13}C_6$, $^2H_7$]glucose, 11.8 T, 40 mM, 40 mOsm, TE	16.6 (14.8, 18.4)	16.9 (16.4, 17.5)	15.9 (15.3. 16.4)	16.1 (14.4, 17.8)	16.0 (13.0, 19.0)	14.3 (14.0, 14.5)	16.2 (15.7, 16.7)	11.4 (11.0, 11.7)
H	[U-$^{13}C_6$, $^2H_7$]glucose, 4.7 T, 400 mM, 400 mOsm, TE	8.2 (7.0, 9.4)	8.4 (7.9, 8.9)		7.0 (3.1, 10.8)			8.0 (5.2, 10.8)	6.2 (6.0 ,6.4)
I	[U-$^{13}C_6$, $^2H_7$]glucose, 3 T, 26 mM, 314 mOsm, HP				9.5 ($\pm$ 0.6)[b]				

[a]95% Confidence interval provided by the curve fitting is shown in brackets.
[b]Mean and standard deviation of three studies as reported in the Experimental section.
TE, Data acquired under thermal equilibrium conditions (see Experimental section). HP, Data acquired at a hyperpolarized state (see Experimental section).

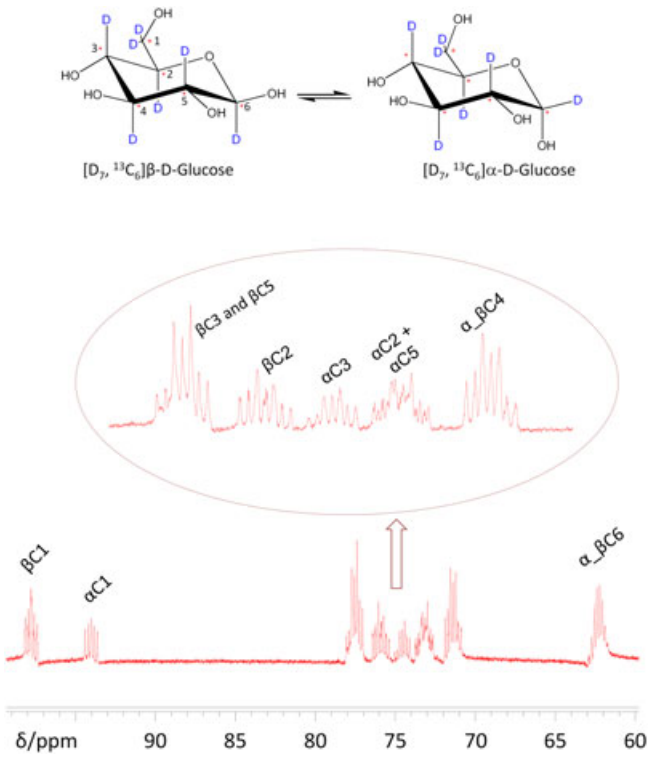

Figure 2. ^{13}C spectrum of [U-$^{13}C_6$, $^{2}H_7$]glucose in water at 11.8 T and 37 °C. Eight groups of signals were assigned to their corresponding carbon positions in the molecule. The structure of the α and β anomers of [U-$^{13}C_6$, $^{2}H_7$]-D-glucose is shown at the top. D, Deuterium atoms; * ^{13}C atoms. The various carbon positions (C_i) are marked by numerals. Heteronuclear irradiation (proton or deuterium) was not applied.

The T_1 of [U-$^{13}C_6$, $^{2}H_7$]glucose at 3 T was found to be 9.5 ± 0.6 s ($n = 3$). In this measurement, the integrated intensity over all of the carbon positions was used owing to the difficulty in resolving the various carbon signal groups in the 3 T spectra. Three hyperpolarized studies were performed in solution, as described in the Experimental section.

Altogether, although [U-$^{13}C_6$, $^{2}H_7$]glucose T_1s were found to vary at different magnetic fields, we could not identify a clear trend for this variation. Because the ability to resolve the individual [U-$^{13}C_6$, $^{2}H_7$]glucose carbons' signals decreases with a decrease in the magnetic field strength, a detailed analysis of the T_1 dependence on magnetic field for each carbon position is not possible with the fully ^{13}C labeled molecule as the signals of the different positions heavily overlap. For this reason the T_1 at 3 T was calculated as an average for the six carbon positions in the α and β anomers together.

2.3. Polarization

The polarization level of [U-$^{13}C_6$, $^{2}H_7$]glucose in the solution in the magnet was $4.2 \pm 0.4\%$ ($n = 3$). We note that the glucose polarization protocol was not optimized and was based on a previously developed polarization protocol for choline analogs (20). It may be that optimization would lead to a higher polarization level. In addition, the transfer time from the polarizer to the magnet (15 ± 2 s) was long compared with the T_1 of the compound (9.5 s at 3 T). Therefore, shortening the transfer time is likely to have a substantial effect on the measured polarization level as well.

Extrapolating back to the point of dissolution at the DNP polarizer, taking into account 15 ± 2 s as the duration between the end of polarization and the measurement in the scanner, the polarization would be $21 \pm 6\%$ in solution at the DNP polarizer immediately after dissolution. It is not possible to account for the effect on the final polarization of variations in magnetic field during transport of the agent from polarizer to MRI scanner; therefore, this represents a lower bound on the error.

2.4. Carbon-13 Dipolar Interactions

To gain maximal signal from hyperpolarized glucose we chose to use a glucose analog that is labeled in all carbon positions. The possible effect of direct carbon-13 to carbon-13 bonding on the individual carbon-13 T_1s was investigated to study the effect of these added dipolar interactions on T_1 relaxation times. To this end, two compounds were investigated: [U-$^{13}C_6$, $^{2}H_7$]glucose and [$^{2}H_7$]glucose at 400 mM, 37 °C and 11.8 T (Fig. 1 and Table 1). While both compounds are fully deuterated, all carbon positions in the [U-$^{13}C_6$, $^{2}H_7$]glucose molecule are 99% occupied by ^{13}C nuclei, while only ca. 1.1% of each carbon position is occupied by ^{13}C nuclei in the [$^{2}H_7$]glucose molecule owing to the naturally abundant distribution of ^{13}C. The chance of having two directly bonded ^{13}C nuclei in the latter molecule is therefore 0.01% (negligible); thus this measurement was indicative of the T_1 of a single ^{13}C-labeled glucose. It was found that the T_1 of glucose ^{13}Cs in a uniformly ^{13}C-labeled glucose was shorter by 3.3 s (8.9 ± 1.4 s vs 12.2 ± 1.3 s, 27% decrease). Therefore, direct bonding of additional ^{13}C nuclei led to a decrease in glucose ^{13}C T_1s, as could be expected owing to the additional dipolar interactions. However, as can be seen in the following, this decrease in T_1 did not prevent imaging of hyperpolarized [U-$^{13}C_6$, $^{2}H_7$]glucose.

The fully deuterated and fully ^{13}C labeled [U-$^{13}C_6$, $^{2}H_7$]glucose has two competing properties in terms of its potential hyperpolarized signal. On one hand, it is labeled at six positions, all with similar T_1. This property can be utilized to increase the initial hyperpolarized signal 6-fold. On the other hand, the T_1s of these carbon-13 nuclei are shorter than any hyperpolarized probe reported to date (17).

2.5. Simulation of Signal Enhancement and Decay

To gain insight into the relative imaging signal increase that would be provided using this glucose analog in a hyperpolarized state, we simulated its signal enhancement and decay, comparing the signal expected from the glucose analog to that of [1-^{13}C]pyruvate (Fig. 3). The latter agent and acquisition approach are considered a 'gold standard' in the field, with known enhancement characteristics (17). In the simulation we considered that: (a) pyruvate is injected at a dose of 0.2 mmol kg^{-1}, as previously described (16), and glucose is injected at a dose of 1.4 mmol kg^{-1}, which is approximately half the dose that is safe for injection in humans, as per the intravenous glucose tolerance test (see Discussion); (b) the initial liquid state polarizations per ^{13}C nucleus (immediately following dissolution) are the same; (c) the T_1 of pyruvate is 55 s (16); (d) the T_1 of glucose is position- and anomer-dependent; and (e) the bandwidth for image acquisition is the same.

Individual position T_1 values (T_{1_ci}), as determined at 7 T, 400 mM and 37 °C, were used in this calculation (8–13 s), assuming that the

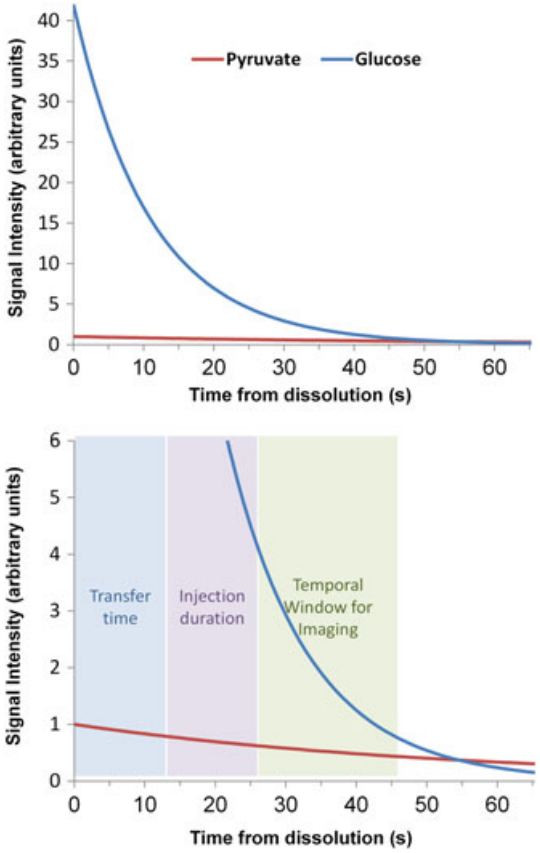

Figure 3. Simulation for the relative imaging signal of hyperpolarized [U-$^{13}C_6$, $^{2}H_7$]glucose compared with hyperpolarized [1-^{13}C]pyruvate. The underlying assumptions for this simulation are described in the text. Individual [U-$^{13}C_6$, $^{2}H_7$]glucose carbon T_1 values, as determined at 7 T, 400 mM and 37 °C, were used in this simulation (see Table 1 and Fig. 1). The lower panel is an expanded version of the upper panel.

α to β anomer ratio is 36:64 (22). The overall glucose signal at a particular time point was calculated as ΣSc_i, where Sc_i is the individual signal for each carbon position at a particular time point. Each Sc_i was calculated according to $Sc_i(t) = I_{SNR} \times \exp(-t/T_{1\_ci})$, where I_{SNR} is the initial signal-to-noise ratio (SNR) or the initial relative imaging signal. The glucose decay curve was normalized to that of pyruvate using the dose ratio, that is, the I_{SNR} of each glucose carbon was taken to be 7-fold that of pyruvate, whereas the latter was set to 1 arbitrary unit.

Considering a duration of approximately 30 s from dissolution start for transfer and injection, this simulation suggests a temporal window for imaging of approximately 25 s, during which the expected signal of hyperpolarized [U-$^{13}C_6$, $^{2}H_7$]glucose is higher than that of hyperpolarized [1-^{13}C]pyruvate (Fig. 3). The simulation also suggests that a remarkable increase in signal may be gained by minimizing the transfer and/or the injection duration.

We note that an imaging signal is always greater than a spectroscopic signal because it integrates over all of the intensities of the injected agent as well as its metabolites. Nevertheless this factor was not taken into account in the simulation because the differences between the total hyperpolarized signal and an individual hyperpolarized metabolite signal are time-dependent and specific to the tissue under investigation, both for glucose and for pyruvate. Therefore, one cannot assign a constant factor for this expected signal increase, although this property is expected to prolong the imaging time window shown in Fig. 3.

2.6. Hyperpolarized Glucose Imaging – *in vitro*

Encouraged by these simulation results, the first hyperpolarized glucose image was recorded at 3 T. A syringe filled with approximately 2.5 ml of hyperpolarized [U-$^{13}C_6$, $^{2}H_7$]glucose solution (104 mM) was placed at the center of the RF coil and the image was recorded within approximately 15–20 s after dissolution (Fig. 4a). Indeed, as expected, the image showed ample signal and very low noise. However, owing to the dispersion of glucose carbons' chemical shifts, several carbon lines are visible. Because the chemical shift dispersion in the glucose spectrum is about 35 ppm (~1120 Hz), the read bandwidth of $\pm$3 kHz is of the order of the chemical shift dispersion, leading to substantial chemical shift artifact. The distance between the most extreme lines in Fig. 4(a) is about 4.5 cm. This is a remarkable presentation of a chemical shift artifact, usually visible on anatomic ^{1}H MRI images in regions with both fat and water. To correct for this artifact, a second image was recorded with a high bandwidth ($\pm$42 kHz). Using these conditions, the individual carbon signals collapsed to yield an artifact-free image with high in-plane resolution and high SNR, despite the loss in SNR at higher bandwidth. This SNR loss was at least partially compensated for by collapsing all the spectral peaks into a single voxel, as seen in Fig. 4(b). In order to calculate the effect of high-bandwidth acquisition on scaling of the total signal in the glucose image, the signal-to-noise in the two images was compared as described in Table 2. The SNR in the low bandwidth image was 5.4×10^5. Because the signal is expected to remain the same and the noise is expected to scale as the square root of the bandwidth, the expected signal-to-noise ratio in the high bandwidth image is 1.4×10^5. The experimental SNR at the high bandwidth image was found to be 1.6×10^5, slightly higher but in agreement with expectations.

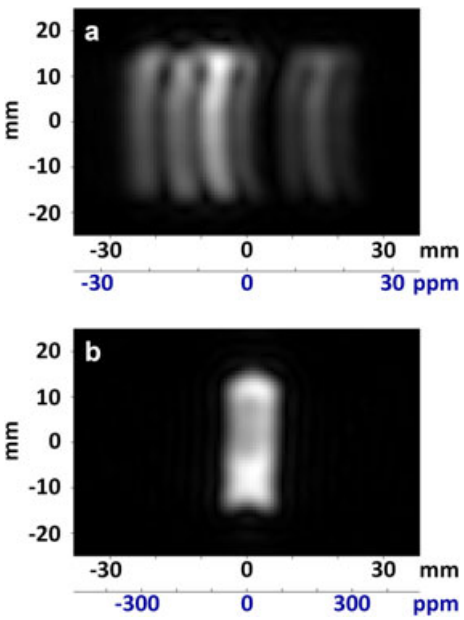

Figure 4. Carbon-13 MRI images of a syringe filled with hyperpolarized [U-$^{13}C_6$, $^{2}H_7$]glucose. Image (a) was recorded with a $\pm$3 kHz bandwidth and demonstrated chemical shift dispersion between the glucose carbons. Image (b) was recorded with a high bandwidth ($\pm$42 kHz) to minimize the chemical shift artifact by collapsing all the carbon chemical shifts to approximately one pixel.

Table 2. Signal-to-noise characteristics of hyperpolarized glucose at low and high bandwidth imaging

	Low bandwidth image	High bandwidth image
Total signal (a.u.)[a]	3.8×10^5	7.2×10^5
Mean signal (a.u.)[b]	133	1075
Real noise (a.u.)[c]	0.7	4.5
Signal-to-noise ratio	$(5.4 \pm 0.1) \times 10^5$	$(1.6 \pm 0.1) \times 10^5$
Band-width (kHz)	±3.01	±41.67

a.u., Arbitrary units.
[a]Total signal is based on the sum of the signal in a region of interest consisting of all visible intensities in the images.
[b]Mean signal represents the mean of the intensities in the same regions of interest.
[c]Noise was based on the standard deviation of the real signal in reference noise scans (no RF).

2.7. Hyperpolarized Glucose Imaging – *in vivo*

As depicted in Fig. 5, hyperpolarized [U-$^{13}C_6$, $^2H_7$]glucose also provided a high signal on carbon-13 images recorded *in vivo*. Normal rats were anesthetized, and hyperpolarized [U-$^{13}C_6$, $^2H_7$]glucose was injected through the tail vein in a bolus of 12 s total duration. Projection images were recorded at 8, 12 and 20 s from the onset of the bolus injection (i.e. during and after the bolus). Each image was acquired within 1 s; three different animals are shown. Cardiac gating was not applied; therefore, each image averages several heart beats.

In the image recorded at 8 s (Fig. 5a), the inferior vena cava and the heart are clearly visible. Arterial hyperpolarized media flow at this time is not likely, as the signal in the kidneys is not yet visible. This image, which was recorded during the bolus at a very high resolution (128 × 128 matrix, in-plane resolution of 1.56 mm), demonstrates the potential of hyperpolarized glucose imaging with regard to angiography. The signal from the injected hyperpolarized media is extremely high with no background signal.

At 12 s (Fig. 5b), at the end of the bolus injection, signal intensity in the main vasculature and the heart is high, with substantial intensity observed in the kidneys. At 20 s from bolus initiation (Fig. 5c), signal from the heart is the most intense signal in the image, about 40% higher than the signal in the vasculature and about 20% higher than the signal in the kidneys. Still, the signal in the kidneys is clearly observed, as well as the signal in other tissues such as the liver.

3. DISCUSSION

The first nonradioactive images of glucose distribution in live rats are presented. Several aspects regarding the current results and suggested applications are discussed below.

3.1. The use of DNP for Imaging of Hyperpolarized Media

DNP hyperpolarization technology has offered the possibility of a new imaging modality ever since it was first described *in vivo* in 2004 (16,23). The main emphasis of this technology thus far has been visualization of actual metabolic conversions *in vivo* (17), with the exception of the very first *in vivo* paper, which used a nonmetabolic compound (23). This property of metabolic visualization is indeed unmatched by any other imaging modality available today. However, we felt that the ample signal provided by hyperpolarization may be advantageous *per se* for monitoring the distribution of metabolically important compounds, even without obtaining information on specific metabolic pathways. Of specific interest are compounds with uptake characteristics that are favorable for identifying pathologies. FDG-PET has already revealed the promise of glucose uptake as a biomarker. For this reason, we have attempted to image glucose with hyperpolarized MRI. Technically, the use of ^{13}C imaging as opposed to spectroscopic imaging, which is usually performed for metabolic analysis, provides a relative increase in SNR (owing to the combined signal of all metabolites) and lowers the demands of nonroutine pulse sequence and reconstruction tools.

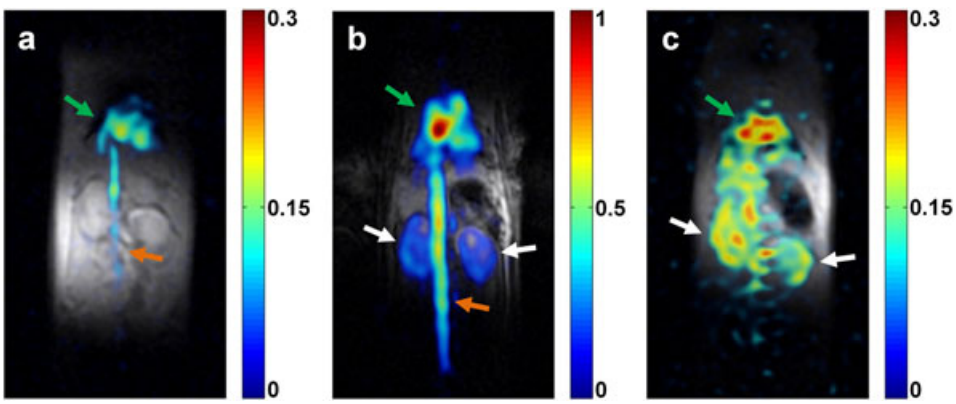

Figure 5. Carbon-13 MRI images of rats injected with hyperpolarized [U-$^{13}C_6$, $^2H_7$]glucose. Images were recorded: (a) during the injection – 8 s from injection start; (b) at the end of the injection – 12 s from injection start; and (c) after the injection – 20 s from injection start, in three different rats. Color hyperpolarized images are presented overlaid on proton images from the same rat. The color scales represent arbitrary linearly distributed intensity units for the hyperpolarized images. Each image is presented with the optimal viewing window and the relative intensities in the three images can be compared based on the corresponding color scale. The hyperpolarized signals in the kidneys and the inferior vena cava are marked with white and orange arrows, respectively. The green arrow points to the hyperpolarized signal in the heart and lungs in (a) and (b) and apparently only the heart in (c). The regions of the head and tail of the rats were outside the field of view of both RF coils – ^1H and ^{13}C.

3.2. SNR – Fully ^{13}C-Labeled Glucose

While the use of fully ^{13}C-labeled glucose has 6-fold SNR per mole compared with a singly ^{13}C labeled molecule, we note that the wide range of chemical shifts dictated a high bandwidth for imaging of ±42 kHz, thus reducing some of the benefit of the increased SNR. It is possible that imaging singly labeled glucose with smaller bandwidth may provide SNR similar to that reported here, but this depends very strongly on the particular conditions of the experiment, including the T_1 values of the particular carbon position selected for labeling (currently unknown at 3 T) and the frequency spread of the ^{13}C signal of that position when metabolized.

3.3. Glucose for DNP – Molecular Agent Life Time and Imaging Time

The ability of a compound to serve as a molecular imaging agent on hyperpolarized MRI is dependent to a great extent on the T_1 of its relevant ^{13}C nucleus or nuclei. We found that substituting directly bonded protons with deuterium atoms led to a significant T_1 prolongation and enabled glucose monitoring in a hyperpolarized state.

The lifetimes demonstrated here for hyperpolarized [U-$^{13}C_6$, $^{2}H_7$] glucose at 3 T were of the order of ~29 s (ca. 3 times the average T_1), which is extremely short compared with the half life of FDG (2 h). Also, the temporal window at which the FDG-PET image is recorded is within 30–60 min from FDG administration. However, a shorter half-life of ca. 2 min was recently reported for an oxygen-15 deoxy-glucose analog, [^{15}O]DG (24). Using this relatively short-lived analog, it was possible with PET imaging to show tissue contrast with regions of high glucose uptake or accumulation such as the brain, heart, kidneys and bladder at high intensity, a contrast pattern that is similar to that of [^{18}F]FDG-PET. This pattern was evident already at 5 min post [^{15}O]DG administration. Importantly, $H_2^{15}O$ administration in the same study showed no specific contrast and a uniform distribution of the label in the body. This study is encouraging in terms of the feasibility of monitoring tissue glucose uptake with a short-lived imaging agent.

3.4. Glucose Uptake and Metabolism

The entire glycolysis pathway, starting from glucose transport and downstream metabolism to CO_2 or ethanol, was recently demonstrated *in vivo* – in yeast – in less than 20 s using the same glucose analog as used here: [U-^{2}H, U-^{13}C] (25). We believe that such a study, which used the same noninvasive technology, that is, NMR spectroscopy, and the same glucose analog, is the most relevant for discussing the rates of glucose metabolism with respect to the time frame of the current experiments.

Transport across the plasma membrane is the first, obligatory step of glucose utilization. Facilitated diffusion-type glucose transport in yeast occurs via the hexose family of transporters, which is composed of at least 20 known genes coding for transport of glucose with a K_m ranging between 1.5 and 100 mM (26). Glucose transport of a facilitated diffusion type in mammalians occurs via the GLUT/SLC2 family of transporters, which is composed of 13 known members. The distribution of the GLUT family members is tissue specific and depends on physiological conditions. The K_m of GLUT_1 and GLUT3 is approximately 1 mM (high affinity) while GLUT 2 has a lower affinity of approximately 15–20 mM. Therefore, similar high-affinity facilitated diffusion glucose transporters are found in yeast as well as in mammals. In the experiments described herein (in mammals), glucose concentration in the blood is high and therefore the facilitated diffusion carriers are likely to be the dominant transport system, as opposed to secondary active glucose co-transport. Assuming that the rate of *in vivo* facilitated diffusion glucose transport is the same in yeast and mammals, we would expect glucose metabolism to occur in mammals at a similar rate to that found in yeast. Therefore, within the experimental time frame of 20 s described herein we would expect glucose metabolism to occur in mammals in general and specifically in the rats that were studied here. We note that glucose metabolites may differ from glucose in their relaxation properties. As we do not know the composition of glucose metabolites in tissue, we cannot speculate on their overall T_1 relaxation behavior. Nevertheless, we note that the end metabolites of glycolysis in mammals, CO_2 and lactate are both compounds with a longer T_1 than glucose. Therefore, decay of the signal owing to metabolism in the tissue is not likely.

Nevertheless, we note that monitoring metabolism was not the purpose of the current study. The most probable tissue in which metabolism would occur would be the heart muscle, which is the only tissue in the anesthetized rat that is expected to show high GLUT1 activity because under anesthesia it is the only active muscle. The brain, which very actively takes up glucose in conscious subjects, as seen on clinical FDG-PET images, actually has very low glucose metabolism under anesthesia, and was therefore not imaged in the present study. Although hyperpolarized spectroscopy had been previously recorded from the heart using hyperpolarized pyruvate (27), we note that such a study requires an experimental protocol that is not straightforward, including: larger animals, dedicated pulse sequences and cardiac gating. Further studies are needed to monitor possible hyperpolarized glucose metabolism in the myocardium or in other tissues.

Although we did not monitor metabolism, the intense hyperpolarized glucose signal observed in the heart at 20 s from bolus start (Fig. 5c) was suggestive of glucose uptake because it was more intense than the signal in the vasculature and the kidneys. We note that heart anatomy cannot be discerned from these hyperpolarized images because the imaging time (1 s) averaged several heart beats (approximately six beats) and cardiac gating was not applied. In addition, signal from hyperpolarized glucose in the blood within the heart could be contributing to this effect. Further studies using MRI techniques that eliminate signal from the blood pool are underway in our team to investigate the possibility that glucose uptake by the myocardium can indeed be determined at short time frames of the order of 20 s.

3.5. Hyperpolarized Glucose MRA

In Fig. 5(a), we show a glucose image obtained as the bolus of hyperpolarized media advances through the inferior vena cava. This image illustrates the usefulness of this imaging approach in catheter angiography. In this application, glucose is used as a safe, high-intensity, injectable agent. At the time this image was recorded, the solution used (53 mg per 4 ml or 68.6 mM) is likely to be diluted by the rat's blood and represents a concentration of <68.6 mM. In the intravenous glucose tolerance test, a bolus of glucose as 300 mg kg^{-1} in a 30% solution (1.67 M), a very high osmolarity medium, is given within 60 s (28). Considering this range of injectable glucose concentrations (68.6–1670 mM) we discuss in the following the signal strength and expected

image contrast that may be obtained clinically. Because MRI resolution is limited by the amount of polarized nuclei per voxel, the possible polarizations of glucose and water are compared. We choose the case in which glucose is injected in an iso-osmotic medium of 300 mM (which equals 300 mOsm).

If hyperpolarized isotopically labeled glucose is injected via a catheter as a solution of ca. 300 mM, the glucose concentration in blood in the immediate proximity of the injection site would be close to 300 mM. We assume a polarization enhancement factor of about 1000 for each of the six carbon-13 nuclei. Such an enhancement at a field of 3 T is expected to lead to a signal level in the vasculature of 1980 M ppm, (0.3 M, thermal polarization for ^{13}C of about 1.1 ppm, an enhancement factor of 1000, and six carbons per molecule). In comparison, the signal level of Gd-enhanced angiography is limited by the amount of polarized water protons (regardless of the amount of Gd-chelate). This polarization at 3 T is about 500 M ppm, (55.5 M, the concentration of water in water is taken as an upper limit for the concentration of water in blood, thermal polarization for ^{1}H of 4.5 ppm, and two protons per molecule). Considering a 4-fold lower SNR for ^{13}C compared with ^{1}H MRI owing to its lower gyromagnetic ratio, the expected hyperpolarized glucose signal is therefore similar to that of thermal equilibrium proton imaging. However, while in Gd-enhanced proton-MR angiography (MRA) the nonenhanced tissue provides a considerable background signal, the lack of background signal in the hyperpolarized application is likely to produce angiographic images with higher contrast-to-noise ratio. In addition, the possibility of injecting hyperosmotic glucose solutions and the potential to reach polarization enhancement factors greater than 1000 may both lead to higher SNR in the hyperpolarized images compared with thermal equilibrium proton imaging.

Glucose MRA could therefore present an alternative to gadolinium contrast-based MRA, particularly for patients at risk of nephrogenic systemic fibrosis, including those with compromised kidney function (29). Glucose MRA could also be an attractive alternative to X-ray or CT angiography, which are associated with high radiation doses for patients, technicians and physicians. We note that the resolution of CT catheter angiography is high, about 0.2–0.25 mm in plane resolution. It remains to be seen whether the added signal owing to high concentration of hyperpolarized [U-$^{13}C_6$, $^{2}H_7$]glucose as a contrast agent could lead to such high resolution in catheter MRA.

Indeed, other compounds such as [^{13}C]urea have been previously suggested as DNP hyperpolarized agents beneficial for angiography (15). Urea has low toxicity for intravenous administration and a similar water solubility to glucose. This makes urea a good candidate for catheter angiography. However, while urea has only one carbon position, glucose has six positions, which offer a 6-fold signal enhancement for very short observation times (assuming their initial polarization level is the same). For immediate observation after release of the contrast medium as requested in catheter angiography, [U-$^{13}C_6$, $^{2}H_7$]glucose appears to be advantageous.

3.6. Safety Profile

When developing molecular imaging agents or contrast agents for clinical use, safety is an issue of utmost importance. In potential clinical applications that are suggested by the current studies in rats, glucose appears to have a uniquely promising safety profile. In clinical practice, the intravenous glucose tolerance test is widely used in the detection of diabetes and insulin resistance, and for investigation of early insulin secretion abnormalities in prediabetic states. It may also be used to test for reactive hypoglycemia and other disorders of carbohydrate metabolism. In such intravenous glucose tolerance tests, a glucose dose of 0.5 g kg^{-1} body weight is administered intravenously in a bolus injection. This dose is safe, and places glucose as one of the safest agents that can be administered intravenously to human subjects. Only about one-quarter of this dose was used in the current study, and human studies may require an even lower dose owing to the generally more active state of the conscious subject compared with the anesthetized rat; however, there is clearly considerable room to increase the dose should additional SNR be required.

3.7. Technological Perspective

Generally, pending proof of efficacy, MRI is an attractive alternative to PET for operational and safety reasons. Using MRI and hyperpolarized glucose analogs may provide alternatives to FDG-PET examination. This new route for glucose imaging could reduce the need for hybrid imaging systems such as PET-CT and PET-MRI because the entire anatomical imaging and functional/uptake/distribution examination can be performed in a conventional MRI scanner equipped with ^{13}C compatible hardware; thus glucose MRI could reduce the cost of such medical imaging applications, if it demonstrates comparable information.

3.8. Clinical Perspective

Tissue uptake of glucose has not been unequivocally demonstrated here. Currently, FDG-PET is mostly focused on oncologic applications, for the identification of primary and metastatic tumors. It remains to be seen whether this new glucose imaging approach could identify primary and metastatic tumors with the same level of confidence as FDG-PET. Nevertheless, in the current study two new applications – glucose MRA and cardiac glucose uptake – have been suggested. We believe that the hyperpolarized MRI approach will open the door to a wide range of glucose imaging studies. These may include studies on infection and inflammation, neurologic and psychiatric conditions, epilepsy, cardiovascular applications, kidney function and numerous other topics currently unforeseen.

3.9. Glucose, Deoxyglucose and other Glucose Derivatives

2-Deoxy-2-fluoro-D-glucose (FDG) at natural abundance, without stable isotope or radioactive labeling, has been used to study deoxy-glucose metabolism by ^{19}F-NMR. The main metabolites found were FDG-6 phosphate (FDG-6-P), its epimer 2-deoxy-2 fluoro-D-mannose-6 phosphate (FDM-6-P), and their nucleoside-di-phosphate (NDP) forms, NDP-FDG and NDP-FDM (30). The limited cellular metabolism of FDG accounts for its inability to leave the cell, which is the basis for determining tissue uptake using FDG. Considering future applications of the approach demonstrated here, it could be advantageous to monitor a glucose derivative that has the same limited metabolic profile using hyperpolarized MRI. Such a derivative would be 2-deoxy-D-glucose that is fully labeled with ^{13}C and labeled with deuterium at all directly bonded proton positions, namely [U-$^{13}C_6$,D_8]-2-deoxy-D-glucose (2DG).

In this respect, we note that the acute toxicity of intravenously injected 2DG was previously investigated in rats: no death was

reported, and there was no change in heart rate or respiratory rate at doses of 0.25, 0.5 or 1 g kg^{-1}. There was a mean decrease in arterial blood pressure at such high doses, but not in a dose-dependent manner (31).

The tissue contrast obtained clinically with radioactive deoxy-glucose in PET images reflects increased deoxy-glucose uptake owing to higher glucose transporter expression, especially GLUT1. Several glucose derivatives, such as deoxy-glucose and glucosamine (e.g. 2-amino-2-deoxy-D-glucose chitosamine) have similar uptake characteristics (32) and may therefore produce similar contrast patterns. Also, further glucosamine olefinic derivatives and ester derivatives on the glucose ring show similar uptake and cellular internalization properties, and may produce similar contrast patterns (33). It is therefore highly likely that [U-$^{13}C_6$, $^{2}H_7$]glucose is taken up into cells by transport systems similar to those used for FDG uptake.

In conclusion, the first nonradioactive images of glucose distribution were obtained in live rats by hyperpolarized MRI. The utility of this imaging approach in catheter angiography was demonstrated by imaging during bolus injection, whereby glucose was utilized as a safe, high-intensity, injectable agent. Hyperpolarized [$^{13}C_6$, $^{2}H_7$]glucose MRI may offer radiation free visualization of glucose uptake in health and disease. Further studies are needed to compare such studies with FDG-PET.

4. EXPERIMENTAL

4.1. Materials

[U-$^{13}C_6$, $^{2}H_7$]glucose and [$^{2}H_7$]glucose were obtained from Cambridge Isotopes Laboratories (Andover, MA, USA). Trityl free radical (OX063) was obtained from GE Healthcare, (London, UK). ProHance was purchased from Bracco Diagnostics Inc. (USA).

4.2. Spectrometers and Scanner

T_1 measurements at ultra high fields (7 and 11.8 T) were carried out using Varian NMR spectrometers (Agilent, Santa Clara CA, USA) located at Hadassah–Hebrew University Medical Center in Jerusalem, Israel. T_1 measurements at 4.7 T were carried out on a Bruker spectrometer (Billerica MA, USA) located at the Technion, Haifa, Israel. Hyperpolarized data were recorded on a 3 T clinical scanner (Discovery MR750, GE Healthcare, Waukesha WI, USA) located at the Robarts Research Institute of the University of Western Ontario, London, Ontario, Canada.

4.3. T_1 analyses at thermal equilibrium

T_1 measurements at thermal equilibrium of ^{13}C nuclei in glucose analogs in a variety of conditions (magnetic field strength, concentration, osmolarity) were performed at 37 °C with the standard inversion recovery pulse sequence. Heteronuclear irradiation (proton or deuterium) was not applied. The data were fitted to equation (1):

$$I = I_0\left[1 - A{*}e^{-t/\tau_1}\right] \quad (1)$$

Curve fitting was carried out using Matlab software (MathWorks Inc., Natick, MA, USA).

4.4. Animals

Male Sprague–Dawley rats weighing approximately 565 ± 64 g ($n = 4$) were acclimatized to the animal housing for a week prior to the study. The rats were fed *ad libitum*. Anesthesia was induced with 5% isoflurane and maintained with 1.5–2.5% isoflurane. All studies were performed under a protocol approved by the University of Western Ontario's Animal Use Subcommittee. Following hyperpolarized studies, rats were sacrificed by isoflurane overdose and intravenous injection of potassium chloride. Hyperpolarized media were injected via a tail vein catheter pre-washed with heparinized saline.

4.5. Hyperpolarization, Dissolution and Injection

A typical preparation for the hyperpolarization experiment is described: [U-$^{13}C_6$, $^{2}H_7$]glucose (80 mg, 414 μmol) was mixed with 100 μl of water containing OX063 14 mM and ProHance 0.7 mM. The contrast agent ProHance was added to the preparations as it was previously shown that the addition of a Gd complex to the solid-state preparation increases the polarization level reached at 3.35 T (34). We have previously shown that, for pyruvate polarization, ProHance is a favorable Gd complex contrast agent because it increased significantly the solid-state polarization (about 40%) but had a very small T_1 shortening effect in solution (<10%) (35). The DNP sample was hyperpolarized in a dissolution DNP polarizer (Hypersense, Oxford Instruments, Abingdon, UK) at 1.4 K, 94.1 GHz and 50 mW as previously described (15).

Dissolution was performed in 4 ml of dissolution medium containing 98 mM sodium chloride in water and 100 mg l^{-1} EDTA. The amount of sodium chloride in the dissolution medium was calculated to complement the glucose concentration to 300 mOsm. A volume of 2.5 ml of this hyperpolarized medium was typically injected into the rat. The bolus injection to the tail vein started typically 15–20 s following dissolution.

4.6. Monitoring of Physiological Parameters

During the injection, an increase in heart beat rate and a decrease in breathing rate were observed and resolved within <1 min. These physiological changes were attributed to the injection of large volume in a short time rather than to the active ingredient in the hyperpolarized media (in the current study, glucose). The rat was warmed to 36–37 °C using a water circulation bath. The body temperature was not continuously monitored.

4.7. MR Imaging and Spectroscopy

MRI was performed in the 3 T clinical MRI scanner (Discovery MR750) equipped with a transmit/receive birdcage ^{13}C RF coil, 10 cm i.d. (Morris Instruments, Ottawa, Ontario, Canada) and a custom-built ^{1}H surface coil that fitted within the ^{13}C coil. The animal was placed in a supine position at the center of the ^{13}C coil and the proton coil was centered underneath the animal's abdomen.

4.8. *In vivo* Hyperpolarized ^{13}C Imaging

Coronal projection ^{13}C imaging was performed using a variable flip angle (36) gradient echo sequence with the following acquisition parameters: acquisition time 1 s, repetition time 17.7 ms, echo time 8.9 ms, readout bandwidth ±42 kHz, centric phase

encoding, matrix size 64 × 64, and a field-of-view 200 × 200 mm. [U-$^{13}C_6$, $^{2}H_7$]glucose was injected as a 12 s bolus (2.5 ml) in each experiment. Images were acquired between 8 and 20 s after the start of the bolus injection. The dose of [U-$^{13}C_6$, $^{2}H_7$]glucose injected was approximately 88 mg kg^{-1} in each injection (50 mg per 565 g).

4.9. Determination of Polarization Level

For determination of polarization level in solution, we used the same solid-state polarization and dissolution protocols that were used in the *in vivo* studies. Within ca. 1 h, the polarization in solid state prior to dissolution reached 83 ± 3% ($n = 3$) of the maximal solid-state polarization level, as calculated by fitting the polarization build-up curve. The enhancement factor and corresponding polarization level in solution at 3 T were measured 15 ± 2 s ($n = 3$) from the moment of obtaining the dissolved hyperpolarized media from the polarizer. This delay was the time required for transport of the hyperpolarized solution from the polarizer to the RF coil inside the MRI system. A series of 128 excitations with a flip angle of 10° and a repetition time of 3.5 s was acquired immediately upon placement of the hyperpolarized media (3.5 ml in a syringe) in the MRI RF coil. The hyperpolarized solution was warmed to approximately 37 °C when dispensed from the polarizer, while the polarization measurements were made at room temperature (about 20 °C), so the sample probably cooled somewhat during the transfer and measurement time. The first spectrum recorded in the magnet was compared with a thermal equilibrium signal of a more concentrated solution (520 mM in 5.6 ml of deionized water, containing 70 µl of ProHance, which consists of 0.5 M Gd complex). The ^{13}C signal of the polarized [U-$^{13}C_6$, $^{2}H_7$]glucose media (26 mM in 314 mOsm NaCl, as above) was too low to be detected at thermal equilibrium. For this reason the hyperpolarized signal was compared with a thermal equilibrium signal of the more concentrated sample (520 mM) that was thermally equilibrated to room temperature. The thermal equilibrium spectrum was acquired with a flip angle of 90°, repetition time of 3.5 s and 1024 excitations. The effect of differences in the number of excitations, flip angle and the amount of [U-$^{13}C_6$, $^{2}H_7$]glucose was taken into account in the calculation of enhancement factors and the corresponding polarization levels.

4.10. Determination of T_1 for [U-$^{13}C_6$, $^{2}H_7$]glucose at 3 T

T_1 measurements in a hyperpolarized state consisted of recording the decay curve of the hyperpolarized signal (acquired as described above, [U-$^{13}C_6$, $^{2}H_7$]glucose, 26 mM in 314 mOsm NaCl). The intensity data were analyzed using the standard decay equation, where the effect of RF pulsation (10°) on the decay rate was taken into account using a point-by-point correction of the data by a factor of 1/cos (10°). This correction factor for T_1 measurement at hyperpolarized state is based on a theory developed by Day *et al*. in 2007 (37), following the initial work by Look and Locker in 1970 (38). The correction factor of 1/cos(10°) was applied to each data point on the decay curve individually rather than as a cumulative correction of 1/cos^n(10°), where n would be the number of pulses applied to the sample until that point. Curve fitting was carried out using Matlab software (The MathWorks Inc., Natick, MA, USA).

Acknowledgements

We thank Shifi Kababya for acquiring inversion recovery data at 4.7 T. We thank Jacob Sosna and Yevgeni Libson for support and useful discussions during the study. We thank Shifra Fraifeld for editing this manuscript. This work was funded by BrainWatch Ltd, the Canada Research Chairs program (C.A.M.), the Ontario Research Fund (C.A.M.), and the Israel Science Foundation (grant no. 284/10 to R.K.B.).

4.11. Declaration of Interests

Rachel Katz-Brull is a shareholder, Hyla Allouche-Arnon a past employee and J. Moshe Gomori a consultant of BrainWatch Ltd.

REFERENCES

1. Pasteur L. *1Germ Theory and its Applications to Medicine & on the Antispetic Principle of the Practice of Surgery, trans*. Joseph Lister. Prometheus Books: New York, 1996.
2. Otto Meyerhof – Biography. *Nobel Lectures, Physiology or Medicine 1922–1941*. Elsevier: Amsterdam, 1965.
3. Vander Heiden MG, Cantley LC, Thompson CB. Understanding the Warburg effect: the metabolic requirements of cell proliferation. Science (New York) 2009;324(5930):1029–1033.
4. Kubota K, Nakamoto Y, Tamaki N, Kanegae K, Fukuda H, Kaneda T, Kitajima K, Tateishi U, Morooka M, Ito K, Minamimoto R, Murakami K. FDG-PET for the diagnosis of fever of unknown origin: a Japanese multi-center study. Ann Nucl Med 2011;25(5):355–364.
5. Garcia-Espinosa MA, Rodriques TB, Sierra A, Benito M, Fonseca C, Gray HL, Bartnik BL, Garcia-Martin ML, Ballesteros P, Cerdan S. Cerebral glucose metabolism and the glutamine cycle as detected by in vivo and in vitro C-13 NMR spectroscopy. Neurochem Int 2004;45(2–3):297–303.
6. Lapidot A, Haber S. Effect of endogenous beta-hydroxybutyrate on brain glucose metabolism in fetuses of diabetic rabbits, studied by (13)C magnetic resonance spectroscopy. Brain Res Dev Brain Res 2002;135(1–2):87–99.
7. Lutz NW, Yahi N, Fantini J, Cozzone PJ. Perturbations of glucose metabolism associated with HIV infection in human intestinal epithelial cells: a multinuclear magnetic resonance spectroscopy study. AIDS 1997;11(2):147–155.
8. Oz G, Seaquist ER, Kumar A, Criego AB, Benedict LE, Rao JP, Henry PG, Van De Moortele PF, Gruetter R. Human brain glycogen content and metabolism: implications on its role in brain energy metabolism. Am J Physiol Endocrinol Metab 2007;292(3):E946–E951.
9. Hausler N, Browning J, Merritt M, Storey C, Milde A, Jeffrey FMH, Sherry AD, Malloy CR, Burgess SC. Effects of insulin and cytosolic redox state on glucose production pathways in the isolated perfused mouse liver measured by integrated H-2 and C-13 NMR. Biochem J 2006;394:465–473.
10. Jin ES, Jones JG, Burgess SC, Merritt ME, Sherry AD, Malloy CR. Comparison of [3,4-C-13(2)]glucose to [6,6-H-2(2)]glucose as a tracer for glucose turnover by nuclear magnetic resonance. Magn Reson Med 2005;53(6):1479–1483.
11. Previs SF, Brunengraber H. Methods for measuring gluconeogenesis in vivo. Curr Opin Clin Nutr Metab Care 1998;1(5):461–465.
12. Bluck LJC, Clapperton AT, Coward WA. C-13- and H-2-labelled glucose compared for minimal model estimates of glucose metabolism in man. Clin Sci 2005;109(6):513–521.
13. Malloy CR, Sherry AD, Jones JG. Measurement of gluconeogenesis and intermediary metabolism using stable isotopes. US Patent, 07256047, 2007.
14. de Graaf RA, Mason GF, Patel AB, Behar KL, Rothman DL. In vivo H-1–C-13-NMR spectroscopy of cerebral metabolism. NMR Biomed 2003;16(6–7):339–357.
15. Ardenkjaer-Larsen JH, Fridlund B, Gram A, Hansson G, Hansson L, Lerche MH, Servin R, Thaning M, Golman K. Increase in signal-to-noise ratio of >10,000 times in liquid-state NMR. Proc Natl Acad Sci USA 2003;100(18):10158–10163.
16. Golman K, in 't Zandt R, Thaning M. Real-time metabolic imaging. Proc Natl Acad Sci USA 2006;103(30):11270–11275.

17. Kurhanewicz J, Vigneron DB, Brindle K, Chekmenev EY, Comment A, Cunningham CH, DeBerardinis RJ, Green GG, Leach MO, Rajan SS, Rizi RR, Ross BD, Warren WS, Malloy CR. Analysis of cancer metabolism by imaging hyperpolarized nuclei: prospects for translation to clinical research. Neoplasia 2011;13(2):81–97.
18. Harada M, Kubo H, Abe T, Maezawa H, Otsuka H. Selection of endogenous C-13 substrates for observation of intracellular metabolism using the dynamic nuclear polarization technique. Jpn J Radiol 2010;28(2):173–179.
19. Allouche-Arnon H, Lerche MH, Karlsson M, Lenkinski RE, Katz-Brull R. Deuteration of a molecular probe for DNP hyperpolarization – a new approach and validation for choline chloride. Contrast Media Mol Imag 2011;6:499–506.
20. Allouche-Arnon H, Gamliel A, Barzilay CM, Nalbandian R, Gomori JM, Karlsson M, Lerche MH, Katz-Brull R. A hyperpolarized choline molecular probe for monitoring acetylcholine synthesis. Contrast Media Mol Imag 2011;6:139–147.
21. Singh J, Daftary A. Iodinated contrast media and their adverse reactions. J Nucl Med Technol 2008;36(2):69.
22. Tvaroska I, Bleha T. Anomeric and exoanomeric effects in carbohydrate-chemistry. Adv Carbohyd Chem Biochem 1989;47:45–123.
23. Johansson E, Mansson S, Wirestam R, Svesson J, Petersson S, Golman K, Stahlberg F. Cerebral perfusion assessment by bolus tracking using hyperpolarized C-13. Magn Reson Med 2004;51 (3):464–472.
24. Yorimitsu H, Murakami Y, Takamatsu H, Nishimura S, Nakamura E. Synthesis and bioimaging of positron-emitting O-15-labeled 2-deoxy-D-glucose of two-minute half-life. Chem Asian J 2007;2 (1):57–65.
25. Meier S, Karlsson M, Jensen PR, Lerche MH, Duus JO. Metabolic pathway visualization in living yeast by DNP-NMR. Mol Biosyst 2011;7 (10):2834–2836.
26. Boles E, Hollenberg CP. The molecular genetics of hexose transport in yeasts. FEMS Microbiol Rev 1997;21(1):85–111.
27. Lau AZ, Chen AP, Ghugre NR, Ramanan V, Lam WW, Connelly KA, Wright GA, Cunningham CH. Rapid multislice imaging of hyperpolarized (13) C pyruvate and bicarbonate in the heart. Magn Reson Med 2010;64 (5):1323–1331.
28. Hahn RG, Ljunggren S, Larsen F, Nystrom T. A simple intravenous glucose tolerance test for assessment of insulin sensitivity. Theor Biol Med Model 2011;8:12.
29. Abu-Alfa AK. Nephrogenic systemic fibrosis and gadolinium-based contrast agents. Adv Chronic Kidney Dis 2011;18(3):188–198.
30. Kanazawa Y, Umayahara K, Shimmura T, Yamashita T. F-19 NMR of 2-Deoxy-2-fluoro-D-glucose for tumor diagnosis in mice. An NDP-bound hexose analog as a new NMR target for imaging. NMR Biomed 1997;10(1):35–41.
31. Vijayaraghavan R, Kumar DEO, Dube SN, Singh R, Pande KS, Bag BC, Kaushik MP, Sekhar K, Dwarakanath BS, Ravindranath T. Acute toxicity and cardio-respiratory effects of 2-deoxy-D-glucose: a promising radio sensitiser. Biomed Environ Sci 2006;19(2):96–103.
32. Uldry M, Ibberson M, Hosokawa M, Thorens B. GLUT2 is a high affinity glucosamine transporter. FEBS Lett 2002;524(1–3):199–203.
33. Reineri F, Santelia D, Viale A, Cerutti E, Poggi L, Tichy T, Premkumar SSD, Gobetto R, Aime S. Para-hydrogenated glucose Derivatives as potential C-13-hyperpolarized probes for magnetic resonance imaging. J Am Chem Soc 2010;132(20):7186–7193.
34. Ardenkjaer-Larsen JH, Macholl S, Johannesson H. Dynamic nuclear polarization with trityls at 1.2 K. App Magn Reson 2008;34 (3–4):509–522.
35. Friesen Waldner L, Scholl T, Chen AP, Rutt B, McKenzie CA. The effects of contrast agents on hyperpolarized [1-13C]-pyruvic acid. Proc Int Soc Magn Reson Med 2010:3263.
36. Santyr GE, Lam WW, Ouriadov A. Rapid and efficient mapping of regional ventilation in the rat lung using hyperpolarized 3He with flip angle variation for offset of RF and relaxation (FAVOR). Magn Reson Med 2008;59(6):1304–1310.
37. Day IJ, Mitchell JC, Snowden MJ, Davis AL. Applications of DNP-NMR for the measurement of heteronuclear T-1 relaxation times. J Magn Reson 2007;187(2):216–224.
38. Look DC, Locker DR. Time saving in measurement of NMR and EPR relaxation times. Rev Sci Instrum 1970;41(2):250–251.